5-21-2018

Implications of Sensor Inconsistencies and Remote Sensing Error in the Use of Small Unmanned Aerial Systems for Generation of Information Products for Agricultural Management

Mac McKee
Utah State University, mac.mckee@usu.edu

Ayman Nassar
Utah State University, aymnassar@gmail.com

Alfonso F. Torres-Rua
Utah State University, alfonso.torres@usu.edu

Mahyar Aboutalebi
Utah State University, mahyar.aboutalebi@gmail.com

William Kustas
USDA ARS

Recommended Citation

Mac McKee, Ayman Nassar, Alfonso Torres-Rua, Mahyar Aboutalebi, and William Kustas "Implications of sensor inconsistencies and remote sensing error in the use of small unmanned aerial systems for generation of information products for agricultural management", Proc. SPIE 10664, Autonomous Air and Ground Sensing Systems for Agricultural Optimization and Phenotyping III, 1066402 (21 May 2018); http://dx.doi.org/10.1117/12.2305826

Implications of sensor inconsistencies and remote sensing error in the use of small unmanned aerial systems for generation of information products for agricultural management

Mac McKee, Ayman Nassar, Alfonso Torres-Rua, Mahyar Aboutalebi, William Kustas

Mac McKee, Ayman Nassar, Alfonso Torres-Rua, Mahyar Aboutalebi, William Kustas, "Implications of sensor inconsistencies and remote sensing error in the use of small unmanned aerial systems for generation of information products for agricultural management," Proc. SPIE 10664, Autonomous Air and Ground Sensing Systems for Agricultural Optimization and Phenotyping III, 1066402 (21 May 2018); doi: 10.1117/12.2305826

SPIE.

Event: SPIE Commercial + Scientific Sensing and Imaging, 2018, Orlando, Florida, United States

Implications of sensor inconsistencies and remote sensing error in the use of small unmanned aerial systems for generation of information products for agricultural management

Mac McKee[1a], Ayman Nassar[a], Alfonso Torres-Rua[a], Mahyar Aboutalebi[a], William Kustas[b]
[a]Utah Water Research Laboratory, Utah State University, Logan, UT, 84322-8200; [b]USDA-ARS Hydrology and Remote Sensing Laboratory, Beltsville, MD, 20705-8431

ABSTRACT

Small, unmanned aerial systems (sUAS) for remote sensing represent a relatively new and growing technology to support decisions for agricultural operations. The size and power limitations of these systems present challenges for the weight, size, and capability of the sensors that can be carried, as well as the geographical coverage that is possible. These factors, together with a lack of standards for sensor technology, its deployment, and data analysis, lead to uncertainties in data quality that can be difficult to detect or characterize. These, in turn, limit comparability between data from different sources and, more importantly, imply limits on the analyses that can be accomplished with the data that are acquired with sUAS. This paper offers a simple statistical examination of the implications toward information products of an array of sensor data uncertainty issues. The analysis relies upon high-resolution data collected in 2016 over a commercial vineyard, located near Lodi, California, for the USDA Agricultural Research Service Grape Remote sensing Atmospheric Profile and Evapotranspiration eXperiment (GRAPEX) Program. A Monte Carlo analysis is offered of how uncertainty in sensor spectral response and/or orthorectification accuracy can affect the estimation of information products of potential interest to growers, as illustrated in the form of common vegetation indices.

Keywords: remote sensing, unmanned autonomous vehicle, spectral response, orthorectification accuracy, uncertainty

1. INTRODUCTION

Unmanned autonomous vehicles (UAVs), or unmanned aerial systems (UASs), or, simply, "drones", have seen extensive use for military applications for many years, but it is only in relatively recent times that they have become commercially available for the domestic market. This includes a growing set of products for use in remote sensing (RS) applications in agriculture. Many of these products rely on data based on certain spectral characteristics of the sensors flown by the UAS and are potentially limited in their repeatability and accuracy by the radiometric and image processing protocols that are used to transform raw imagery into scientific data. Entry costs for companies that seek to market RS products for use in agriculture are relatively low, and there are few standards in place for performance of sensors, planar accuracy of orthomosaics, etc. This means that, in the context of the current market, there is a diversity of cameras and sensors, image processing software, field protocols, and so forth, available for sale, resulting in a poorly understood range of positional accuracy and radiometric performance of RS products. Further, there is growing interest in "precision agriculture" and the role that UAS-based RS can play in it. This will place greater importance on accuracy, repeatability, and comparability of the RS data, both at UAS and satellite resolutions, and on the analytic efforts used in support of management decisions of growers engaged in precision agriculture. However, the impact on the quality of RS products in terms of the range of uncertainty in spectral and image processing performance of the array of technologies for UAS RS is not fully explored. This paper examines this issue through application of Monte Carlo methods using high-quality, high-resolution multispectral imagery of a wine grape vineyard acquired near Lodi, California. These data were collected and processed by the AggieAir™ remote sensing group [1] at Utah State University in cooperation with the USDA Agricultural Research Service Grape Remote sensing Atmospheric Profile and Evapotranspiration eXperiment (GRAPeX) Program. Specifically, the effects of uncertainty in sensor spectral response and horizontal error in the geolocation of individual pixels are explored in terms of their impact on the estimate of two standard vegetation indices, normalized difference vegetation index (NDVI) and vegetation health index (VHI).

[1] mac.mckee@usu.edu; phone 1-435-797-3188

Autonomous Air and Ground Sensing Systems for Agricultural Optimization and Phenotyping III, edited by J. Alex Thomasson, Mac McKee, Robert J. Moorhead, Proc. of SPIE Vol. 10664, 1066402
 · doi: 10.1117/12.2305826

1.1 Sensor spectral response uncertainty

Digital cameras utilize arrays of detectors that each sense incident electromagnetic energy in a particular range of wavelengths and translate this signal into an electrical current. An array of such detectors is called a focal plane array (FPA), and usually contains millions to tens of millions of detectors arranged in a rectangular grid. When an image is acquired, the camera transforms the electrical output from each of the millions of detectors into individual pixel values, each of which is an integer. These integer values, called "digital numbers", or DNs, are often represented in 8-, 12-, or 14-bit format. These DNs are not a direct measure the energy reflected from the surface, yet most RS applications require that a measurement of reflected electromagnetic energy be used to support any number of scientific calculations that provide a description of surface phenomena observed in the imagery. The precise nature of the transformation from DNs to a measure of reflected electromagnetic energy is called the spectral response function (SRF) of the sensor. Even things as simple as basic vegetation indices must be based on such measurements of reflected electromagnetic energy. (Refer to [2] for a much more detailed and informative introduction to the topic of spectral response functions.)

Studies done with RS data produced by satellite platforms carrying high-quality sensors have shown that data derived from different sensors can yield quite different characterizations of surface conditions. An examination of the effects of the spectral response of several advanced, very high-resolution radiometers aboard several different moderate-resolution satellites showed that, for identical atmospheric conditions and similar surface reflectance conditions, the spectral reflectance data and calculated NDVI values were sensitive to the SRFs of the various sensors [3]. Variations in the SRF have been recognized as one of the most important sources of uncertainty for the use of RS imagery [4]. In this study, differences were observed in the SRF of 21 earth observation satellite sensors for red, near infrared, and shortwave infrared reflectances and resulting NDVI values. These results indicate that reflectances and NDVI from different satellite sensors cannot be regarded as equivalent. The authors of [4] also contend that variations in processing strategies and algorithm preferences among sensor systems and data streams "…hinder cross-sensor spectra and NDVI comparability and continuity."

The DNs generated by the individual sensors in a FPA must be converted to estimates of the energy reflected from the surface. The process by which this is accomplished is called radiometric calibration. This sequence of events involved with collection of scientific data, from the selection of cameras, lenses, and optical filters, to the protocols followed in image acquisition and radiometric calibration, introduces uncertainties in the RS data that results. These uncertainties arise in different ways, including:

- Different sensors/cameras/lenses/optical filters have different responses in the same wavelengths (for example, see Figure 1). This will produce differences in the values of various vegetation indices, even when using different sensors of high quality and relatively narrow spectral bands [5].

- Sun, slope, and aspect angles can have a significant effect on pixel DN values [6].

- If not properly addressed, differences in the content of water vapor, aerosols, particulates, etc., of the air column between the sensor and the ground can introduce error into the radiometric calibration results [2], especially for microbolometer thermal cameras [7].

1.2 Orthorectification uncertainty

Orthorectification is the process by which RS imagery is stitched together into a mosaic wherein an estimate of the geolocation of each pixel, both in the horizontal (or "planar") and vertical, is obtained. All orthorectification approaches will produce some amount of error in this horizontal and vertical estimate. Much work has been done in satellite image orthorectification, which typically benefits from high accuracy in the estimation of satellite position and orientation and from the relatively large footprint size of an image. Sub-pixel planar error, as measured by root-mean-squared error (RMSE) was reported in [8]. The influence of digital elevation model (DEM) quality on orthorectification accuracy of forest maps using TerraSAR-X images was explored by [9]. An assessment of different sensor models to achieve the best geometric accuracy in orthorectified imagery products obtained from IKONOS Geo Ortho Kit and QuickBird basic

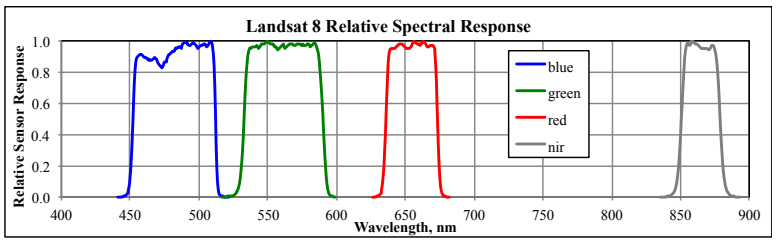

(a)

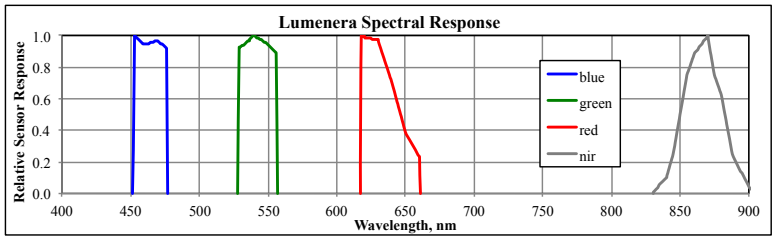

(b)

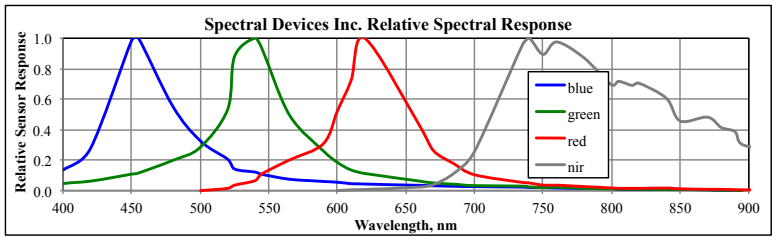

(c)

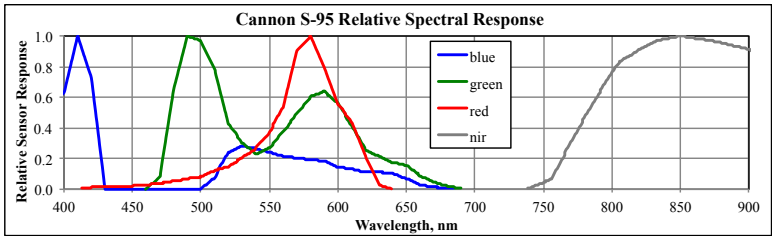

(d)

Figure 1: Examples of Relative Spectral Response of Different Cameras in the Blue, Green Red, and Near Infrared Bands: (a) Landsat 8; (b) Lumenera RGB equipped with narrow-pass optical filters and Lumenera monochrome equipped with narrow-pass near infrared filter; (c) Adapted from Data Shown by Spectral Devices Inc. [10]; (d) Cannon S-95 RGB and Cannon S-95 equipped with wide-band near infrared filter

imagery was explored by [10]. In this study, positional error on the order of one to two meters was reported possible, depending on the orthorectification estimation model selected and the number of ground control points used. A fast and accurate method is reported by [12], capable of automatically selecting and matching a large amount of ground control regions. In this study, the accuracy of the method was assessed using Formosat-2 imagery, and reported RMSE of less than 1.5 pixels. Formosat-2 has spatial resolution of approximately 2 meters.

However, UAS-based RS presents an array of challenges for accurate orthorectification that differ from those of satellites. Most software used for orthorectification of imagery from sUAS is based on fundamental photogrammetric algorithms and pattern recognition. These, in part, normally use information about the position and orientation of the UAS when any given image was acquired. However, the relatively inexpensive global positioning system (GPS) receivers and inertial measurement units (IMUs) available for use on sUAS have limited accuracy in determining the aircraft position and orientation. Error in these measurements, especially with respect to pitch, yaw, and roll from the IMU, can result in substantial error in the estimate of the geolocation of the image. Further, this error grows as sUAS elevation increases.

Challenges associated with orthorectification accuracy of sUAS RS imagery also include the relatively small image footprints, significant image distortion due to the use of low-cost digital cameras, difficulty in locating ground control points, and inaccuracies in automatic tie point generation between images. Some work has been done in improving the accuracy of the orthorectification of UAS-based hyperspectral push-broom imagery using orthosmosaics from frame cameras [13-14]. A semi-automated orthorectification procedure is reported [15] wherein a geometric accuracy of 1.5 to 2 m for imagery of 8 cm resolution was achieved over a limited acreage. In a related study, a RMSE of 48 cm was reported for imagery having approximately 5-cm resolution [16]. A new orthorectification scheme can reportedly achieve 0.33 pixels of accuracy, though the sensors employed in the study limited these results to elevations below 400 m above ground [17].

Fundamentally, orthorectification accuracy cannot be assessed without testing the estimated location of points in the orthomosaic against points on the ground whose locations are accurately known. Commercially available orthorectification services sometimes claim that the planar accuracy "could be as good as plus/minus 3 pixels", which, of course, only places a lower bound on the error and does not provide an estimate of the actual planar positional error in any given orthomosaic.

Error in the estimation of the geolocation of information in an orthomosaic might or might not be important for farm operations, depending on the operational task at hand. Certainly, in the case of precision agricultural activities involving location-aware robotic equipment, there are implications for accuracy and, perhaps, even safety. However, possibly more significant is that fact that positional error limits the collection of accurately georectified data through time in the outcome of operations for purposes of studying trends throughout the growing season or from year to year.

1.3 Objective

The objective of this paper is to explore how uncertainty generated from data from different sensors and imagery having different, and usually unknown amounts of uncertainty in geopositional error, will introduce uncertainty in information derived from the data in the imagery. Measures of the impact of uncertainty in sensor spectral performance and pixel geopositional error is examined in terms of the impact on two, simple vegetation indices: normalized difference vegetation index (NDVI) and vegetation health index (VHI).

2. METHODS AND PROCEDURES

2.1 Study area

As illustrated in Figure 2, the study area consists of a portion of a wine grape vineyard located near Lodi, California. The vineyard (owned by McMannis Winery) is managed by Pacific Agri-Lands Management and, in cooperation with E&J Gallo Winery, has been used as a study site by the Grape Remote sensing Atmospheric Profile and Evapotranspiration eXperiment (GRAPeX) program for several years. GRAPeX is a collaboration of the Agricultural Research Service in USDA, E&J Gallo Winery, Utah State University, and others. High resolution, multispectral imagery has been acquired for the entire vineyard on many occasions for several growing seasons. Multispectral imagery in the red and near infrared bands, illustrated in Figure 1.b, were acquired at 10-cm resolution on May 2, 2016, and are used in this study. Surface temperature data at 60-cm resolution, developed from imagery acquired with a microbolometer camera during the same flight and radiometrically calibrated using procedures reported in [7], are also used. The imagery used in this study is all from the approximately 160-m by 440-m rectangular area shown in Figure 2, which represents something more than 7,000,000 pixels in the red and near infrared bands, and nearly 200,000 pixels in the thermal band. The radiometric data recorded in these bands in the orthomosaic developed from the May 2, 2016 flight will be used as "true" measurements of surface reflectance in the Monte Carlo analyses that are discussed in a subsequent section of this paper.

2.2 Calculation of vegetation indices

To characterize the effects of uncertainty in the consistency of spectral measurements made with different sensors and calibration procedures, as well as uncertainty in the geoposition of any given pixel in a calibrated orthomosaic, two simple but commonly used vegetation indices are used in this paper: normalized difference vegetation index and vegetation health index.

2.2.1 Normalized difference vegetation index

The normalized difference vegetation index (NDVI) used here is of the most common form involving the spectral reflectance values of the red (ρ_{red}) and near infrared (ρ_{nir}) bands, as shown in Equation [1]:

$$NDVI = \frac{\rho_{nir} - \rho_{red}}{\rho_{nir} + \rho_{red}} \quad [1]$$

NDVI is commonly used as an indicator of vegetation condition, with lower NDVI values associated with problems such as lack of soil fertility, pest or disease infestation, or low soil moisture. It is sometimes used as an input to energy balance models of evapotranspiration that are based on data from RS sources.

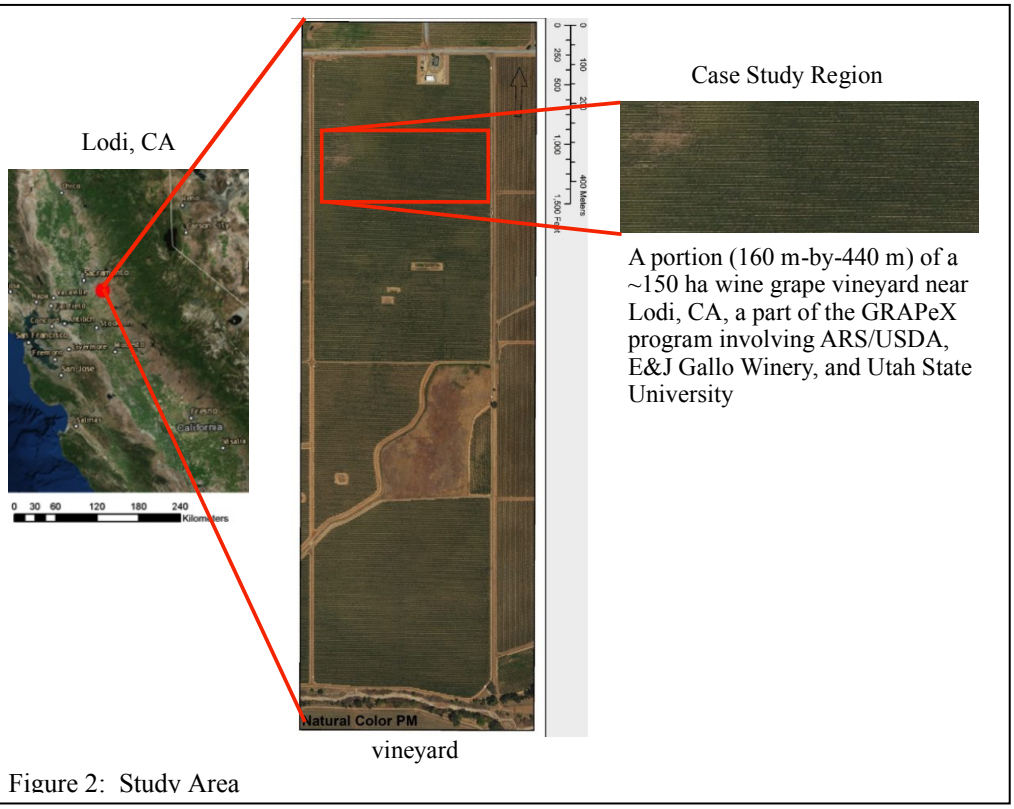

Figure 2: Study Area

2.2.2 Vegetation health index

The vegetation health index (VHI) is a proxy characterizing vegetation health or a combined estimate of moisture and thermal vegetation stress conditions. It consists of a weighted average of a normalized value of NDVI, called the vegetation condition index (VCI), and a normalized temperature index called the temperature condition index (TCI). These indices are shown in Equations [2] and [3], respectively:

$$VCI = \frac{NDVI - NDVI_{min}}{NDVI_{max} + NDVI_{min}} \quad [2]$$

$$TCI = \frac{T_{max} - T}{T_{max} + T_{min}} \quad [3]$$

VHI, then, is expressed as a weighted average of VCI and TCI, as in Equation [4]:

$$VHI = \alpha\, VCI + (1 - \alpha)\, TCI \quad [4]$$

where α must lie between 0 and 1. For purposes of this study, $\alpha = 0.5$.

2.3 Monte Carlo representations

The Monte Carlo analysis involves the random selection of 1,000,000 pixels from the more than 7,000,000 pixels available from the data contained in the rectangular area of the orthomosaic of the Lodi vineyard shown in Figure 2. Each of these pixels was randomly selected by generating uniform, independent deviates across the length and width of the rectangular area. The spectral information and the geolocation of each such selected pixel are considered to be "true" measurements with no error in them. Random deviations of the "true" spectral information from a selected pixel are used to examine the impact of uncertainty in sensor spectral performance. Similarly, spectral information from a nearby pixel that is identified at random with respect to the location of a "true" pixel is used to evaluate the effect of positional uncertainty. Finally, the effect of both positional and spectral uncertainty is evaluated by combining a random positional deviation from the "true" pixel with a random spectral error from the pixel at this "false" location. The following sections provide a description of how these calculations are done.

2.3.1 Monte Carlo model of pixel positional uncertainty

The Monte Carlo representation of pixel positional uncertainty is produced by following these steps:

1. Select a random "true" pixel from the rectangular mosaic of the case study region illustrated in Figure 2. Call this pixel location P. The "true" reflectance and temperature values from this pixel are defined as the vector $\mathbf{R}_{true} = <\rho_{red}, \rho_{nir}, \rho_{temp}>_{true}$.

2. Generate independent displacements Δx and Δy from the location of the "true" pixel, and call this location P_D. These displacements are normally distributed with mean of zero and variance such that Δx and $\Delta y < 3$ meters.

3. Call the pixel reflectance/temperature values found at this new point $\mathbf{R}_{\mathbf{D}} = <\rho_{red}, \rho_{nir}, \rho_{temp}>_{\mathbf{D}}$.

4. Calculate NDVI and VHI values from the reflectance values at these two points, and call them $NDVI_{true}$, VHI_{true}, $NDVI_D$, and VHI_D.

These steps are illustrated in Figure 3. Note that the assumption of a normal distribution of error in each planar direction with a vanishingly small probability at a distance of 3 meters from a selected location is simply a convenience for purposes of this paper. No study has been conducted of what such a distribution should be, and any alternative distribution could be substituted if data to support such a condition could be developed.

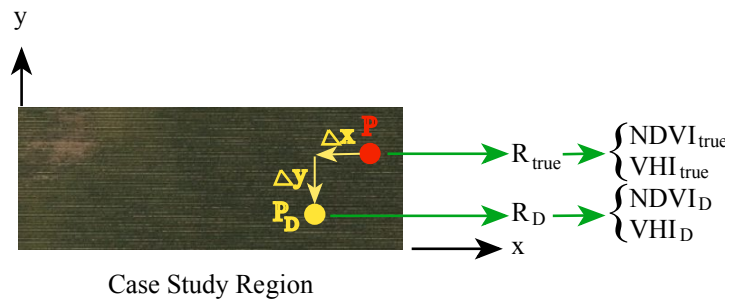

Figure 3: Monte Carlo Representation of the Impact of Spatial Uncertainty

2.3.2 Monte Carlo model of spectral uncertainty

Uncertainty in sensor spectral performance is modeled in this paper as a random deviate that is independently and uniformly distributed between -10% and +10% of the "true" value for the red and near infrared bands, and between -5° C and +5° C for the thermal. As in the case of the introduction of random planar positional uncertainty, these assumptions about the distribution of spectral uncertainty are arbitrary, though, perhaps, reasonable from the point of view of practical experience of the authors. Different distributions could easily be considered. The following steps are used for calculating the effects of spectral uncertainty:

1. Recall the "true" pixel randomly selected within the study area at location P, and its reflectance and temperature values, $\mathbf{R}_{true} = <\rho_{red}, \rho_{nir}, \rho_{temp}>_{true}$.

2. Using the uniform distributions discussed above, generate independent uniform deviates from these "true" reflectance/temperature values, and call them $\mathbf{R}_S = <\rho_{red}, \rho_{nir}, \rho_{temp}>_S$.

3. Similarly, use these same deviations to transform the spectral reflectance/temperature values found at the displaced point P_D, and call them $\mathbf{R}_{DS} = <\rho_{red}, \rho_{nir}, \rho_{temp}>_{DS}$.

4. From these newly created reflectance and temperature values, calculate $NDVI_S$, $NDVI_{DS}$, VHI_S, and VHI_{DS}.

These steps are illustrated in Figure 4. Note that the calculations of $NDVI_{DS}$ and VHI_{DS} represent the combined effects of uncertainty in planar location and spectral performance.

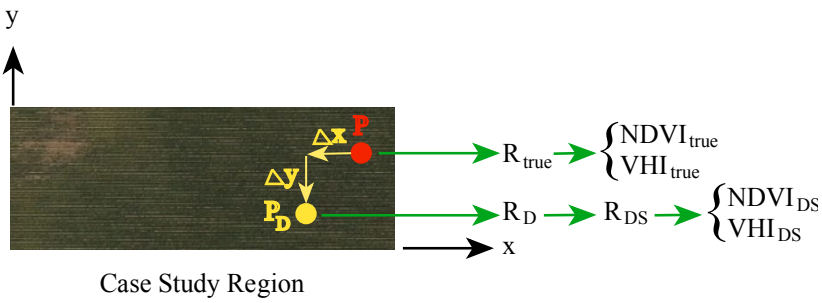

Figure 4: Monte Carlo Representation of the Impact of Spectral Uncertainty and Combined Spatial and Spectral Uncertainty

3. MONTE CARLO SIMULATION RESULTS

3.1 Impact of uncertainty in pixel location

Figures 5.a through 5.d illustrate the uncertainty in NDVI values that results from uncertainty in the accuracy of geolocation of a randomly selected pixel. These figures plot $NDVI_D$ versus $NDVI_{true}$. Figure 5.a represents the results of the least uncertainty in pixel geolocation, and Figure 5.d represents the outcome of much greater uncertainty in geolocation as modeled in the Monte Carlo process. Clearly, uncertainty in NDVI value increases rapidly with increasing error in the estimate of pixel geoposition. At a planar positional uncertainty of less than 0.3 m, the range of $NDVI_D$ values can be as much as approximately 50 percent of the "true" value. This is potentially significant since this planar locational uncertainty for the 10-cm pixels used as the "true" locations is less than three pixels.

Figures 6.a through 6.d show the uncertainty in VHI values that result from positional uncertainty. These results are similar to those seen in the corresponding NDVI plots. Again, fairly significant uncertainty in VHI values develops at a planar positional uncertainty of less than 30-cm, or, in the case of the "true" imagery used in the Monte Carlo analysis, less than three pixels.

3.2 Impact of uncertainty in spectral performance

Figures 7.a through 7.d show the range in estimated NDVI value as a function of uncertainty in spectral performance of the sensor. These are expressed in terms of different ranges of uncertainty in the near infrared band. Clearly, uncertainty in NDVI values is extremely sensitive to spectral uncertainty. Further, the simple nonlinearity in the formula for calculating NDVI leads to a nonlinear response in this uncertainty.

Figures 8.a through 8.d illustrate how uncertainty in VHI might occur as a function of uncertainty in sensor spectral performance. Though VHI is a nonlinear function of spectral and temperature measurements, these responses appear to be somewhat more linear than those of NDVI. However, the range of uncertainty is significant, even at very low deviations from the "true" spectral values.

3.3 Impact of combined positional and spectral uncertainties

When uncertainties in both planar location and spectral response are combined, the resulting uncertainty in vegetation indices becomes dramatic. Figures 9.a through 9.c illustrate this response for NDVI, and Figures 10.a through 10.c show the same for VHI. These are differentiated with respect to planar positional uncertainty. In all cases, an apparent linear trend exists between estimated NDVI/VHI and their corresponding "true" values, but the scatter is very large.

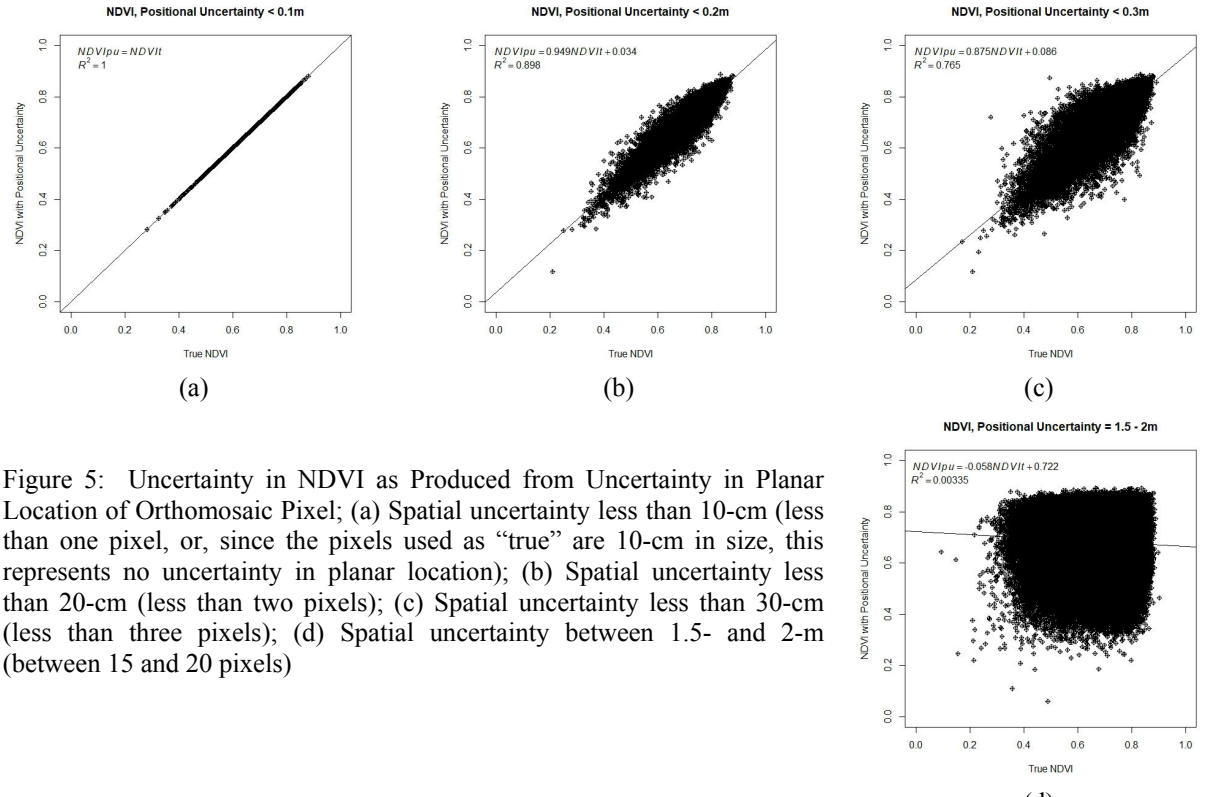

Figure 5: Uncertainty in NDVI as Produced from Uncertainty in Planar Location of Orthomosaic Pixel; (a) Spatial uncertainty less than 10-cm (less than one pixel, or, since the pixels used as "true" are 10-cm in size, this represents no uncertainty in planar location); (b) Spatial uncertainty less than 20-cm (less than two pixels); (c) Spatial uncertainty less than 30-cm (less than three pixels); (d) Spatial uncertainty between 1.5- and 2-m (between 15 and 20 pixels)

4. CONCLUSIONS

This paper presents the results of a Monte Carlo analysis to examine the uncertainty that might result in two conventional vegetation indices, NDVI and VHI, from uncertainty in the estimated planar location of a pixel in an orthomosaic and from uncertainty in the combined spectral response of sensor and radiometric calibration procedures.

With respect to the uncertainty in vegetative indices caused by positional uncertainty in the RS imagery, the differences between "true" and remotely sensed values of NDVI and VHI become significant at a positional error of about two or three pixels, with uncertainties of approximately 40 to 50 percent of the "true" index value. In terms of the effects of spectral uncertainty, similar, or even grater ranges in uncertainty in both NDVI and VHI were found. The effects of combined positional and spectral uncertainty, uncertainty in both NDVI and VHI dominate the index signal, and it is questionable whether there is any useful information contained in the RS product from the point of view of inter-sensor comparison of imagery and comparison of imagery, even from the same sensor, through time.

These behaviors point strongly toward a need for caution when comparing remote sensing results across sensor types and calibration procedures, and through time. This will become much more treacherous for RS products that are more complex and nonlinear, e.g., estimation of evapotranspiration, as opposed to the simple vegetation indices used in this paper.

Researchers and agricultural operators are quite likely to encounter further, more complicated challenges when addressing issues such as differences in spatial resolution, surface heterogeneities that become more apparent at high resolution, shadows, etc.

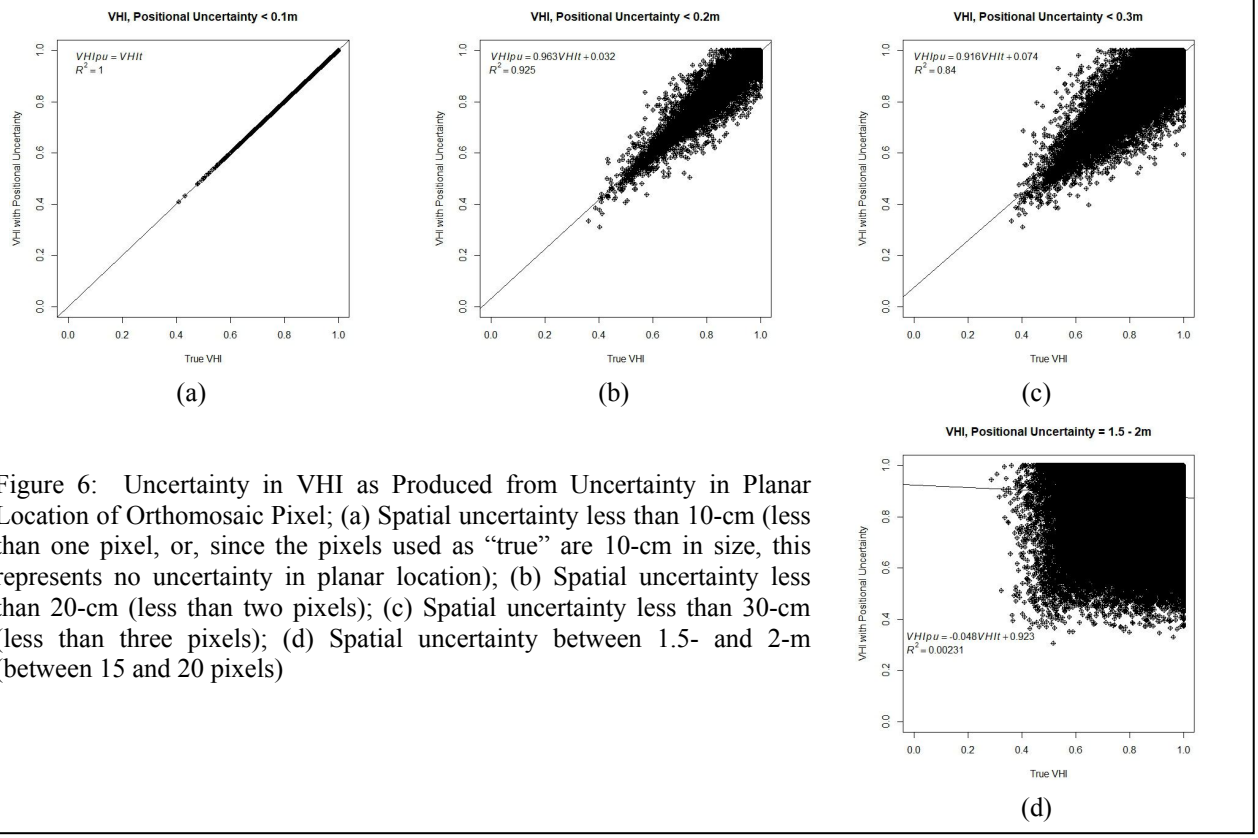

Figure 6: Uncertainty in VHI as Produced from Uncertainty in Planar Location of Orthomosaic Pixel; (a) Spatial uncertainty less than 10-cm (less than one pixel, or, since the pixels used as "true" are 10-cm in size, this represents no uncertainty in planar location); (b) Spatial uncertainty less than 20-cm (less than two pixels); (c) Spatial uncertainty less than 30-cm (less than three pixels); (d) Spatial uncertainty between 1.5- and 2-m (between 15 and 20 pixels)

It should be noted that the Monte Carlo procedure followed in this study has limitations: the probability distributions used to represent uncertainties in planar positional accuracy and estimated radiometric values seem reasonable but are not based on a detailed study of the actual distributions. Further, the selected study area presents very significant challenges to such procedures when applied at the high spatial resolution (10-cm) used in this study of a wine grape vineyard. At this resolution, the imagery shows very large heterogeneity in the vine canopy, itself, and the heterogeneity imposed by the structure of rows of dense vine biomass and widely spaced inter-rows with senescent cover crop and bare soil (during the main growing season) is also a challenge to RS. The range of uncertainties in the vegetative indices used here would almost certainly not be as severe in many other agricultural settings. None-the-less, the magnitude of the uncertainties produced seems significant, especially when discussing opportunities for precision agriculture and the use of robotics equipment to conduct precision farming operations. The agricultural community should be cautiously aware of these issues as sUAS RS technology becomes more available for applications in farm operations.

5. ACKNOWLEDGMENTS

The authors gratefully acknowledge the more than 100 students and faculty collaborators who have participated over the past 12 years in the AggieAir research unit at Utah State University that developed the technology that made possible the acquisition of the base imagery used in this paper. These young geniuses can accomplish anything. The extremely valuable, multi-year collaborative partnership that Utah State University and AggieAir have had with the USDA-ARS Hydrology and Remote Sensing Lab in Beltsville, Maryland, and with the research group at E&J Gallo Winery in

Modesto, California, must also be acknowledged with much gratitude. The brilliant and dedicated scientists in these organizations have helped make AggieAir personnel and technology far better at remote sensing than they otherwise would have been.

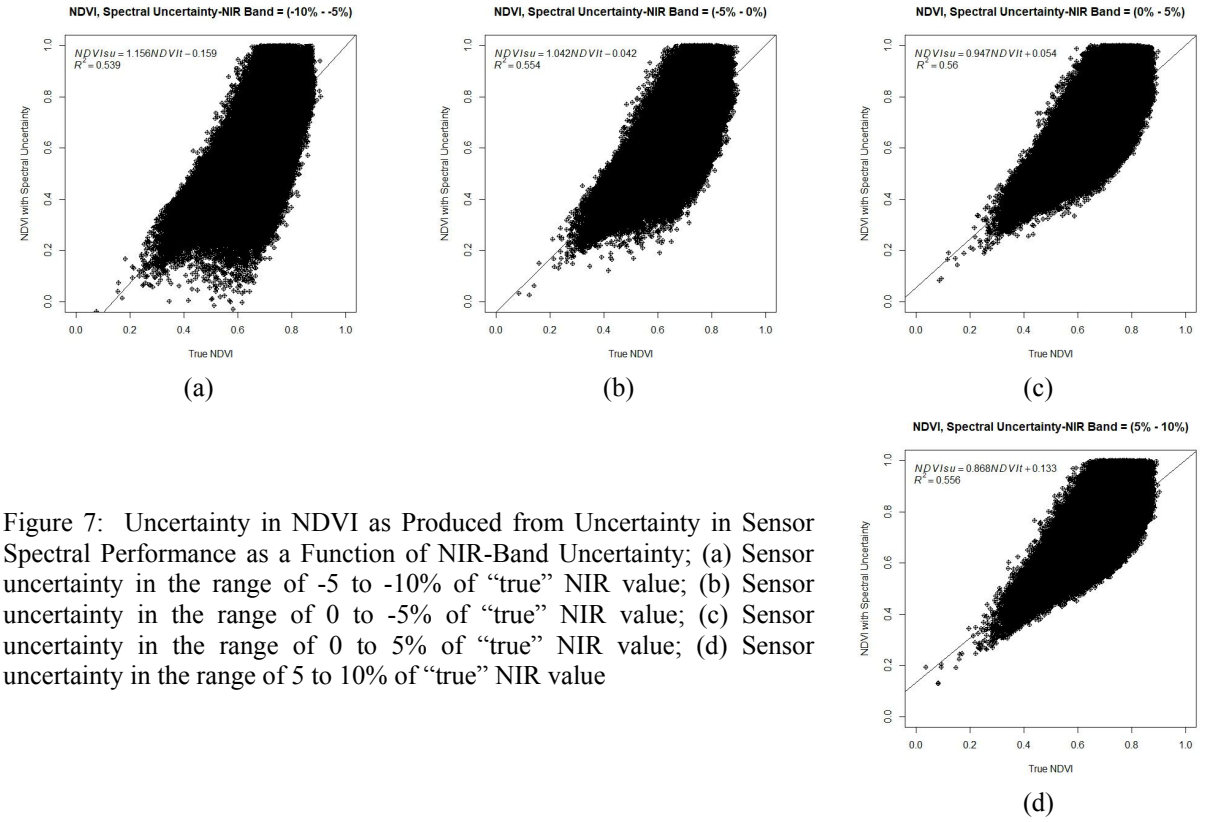

Figure 7: Uncertainty in NDVI as Produced from Uncertainty in Sensor Spectral Performance as a Function of NIR-Band Uncertainty; (a) Sensor uncertainty in the range of -5 to -10% of "true" NIR value; (b) Sensor uncertainty in the range of 0 to -5% of "true" NIR value; (c) Sensor uncertainty in the range of 0 to 5% of "true" NIR value; (d) Sensor uncertainty in the range of 5 to 10% of "true" NIR value

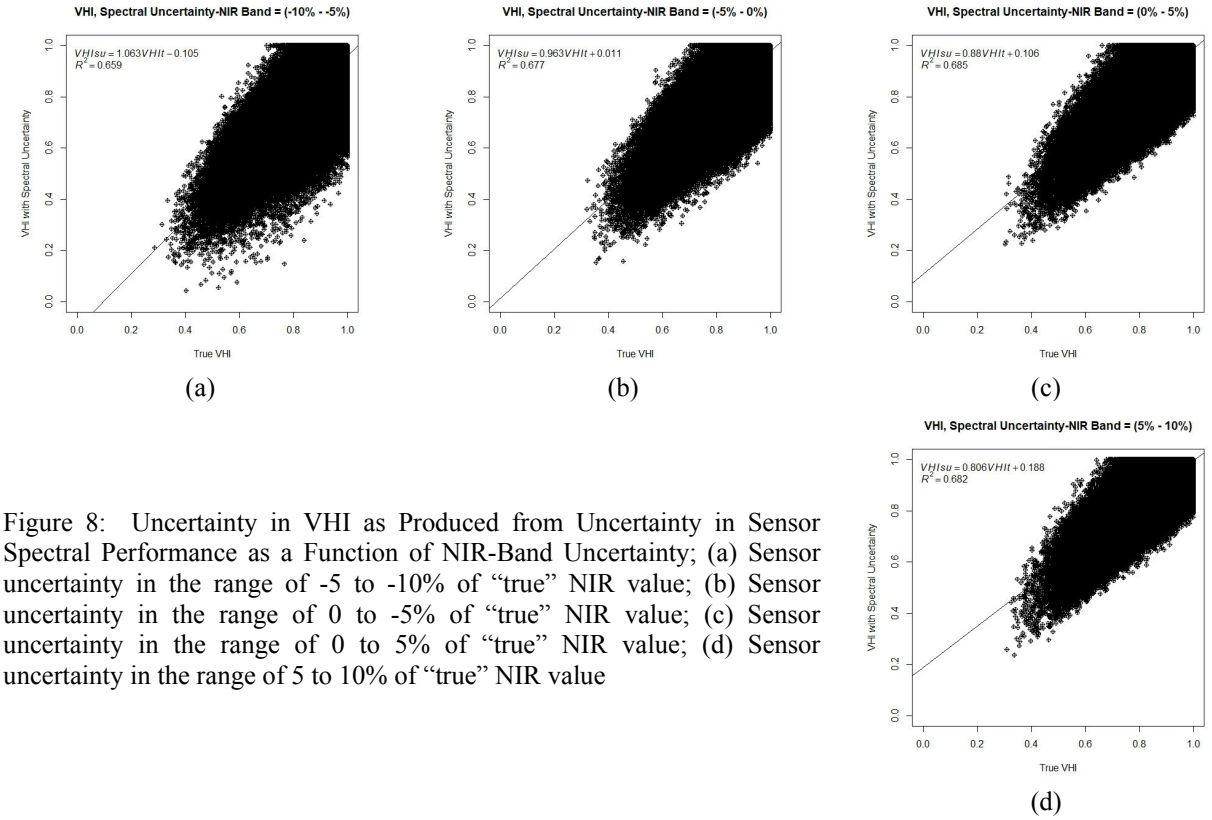

Figure 8: Uncertainty in VHI as Produced from Uncertainty in Sensor Spectral Performance as a Function of NIR-Band Uncertainty; (a) Sensor uncertainty in the range of -5 to -10% of "true" NIR value; (b) Sensor uncertainty in the range of 0 to -5% of "true" NIR value; (c) Sensor uncertainty in the range of 0 to 5% of "true" NIR value; (d) Sensor uncertainty in the range of 5 to 10% of "true" NIR value

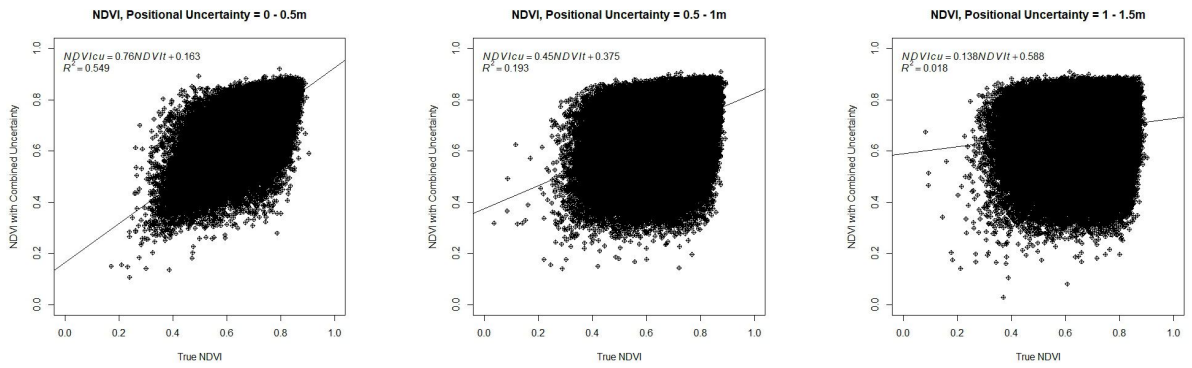

(a) (b) (c)

Figure 9: Uncertainty in NDVI Resulting from the Combined Uncertainty in Planar Geolocation and Sensor Spectral Performance, Shown as a Function of Uncertainty in Planar Geolocation; (a) Planar location uncertainty in the range of 0 to 0.5-m of "true" geolocation (or 0 to 5 pixels); (b) Planar location uncertainty in the range of 0.5- to 1-m of "true" geolocation (or 5 to 10 pixels); (c) Planar location uncertainty in the range of 1- to 1.5-m of "true" geolocation (or 15 to 20 pixels)

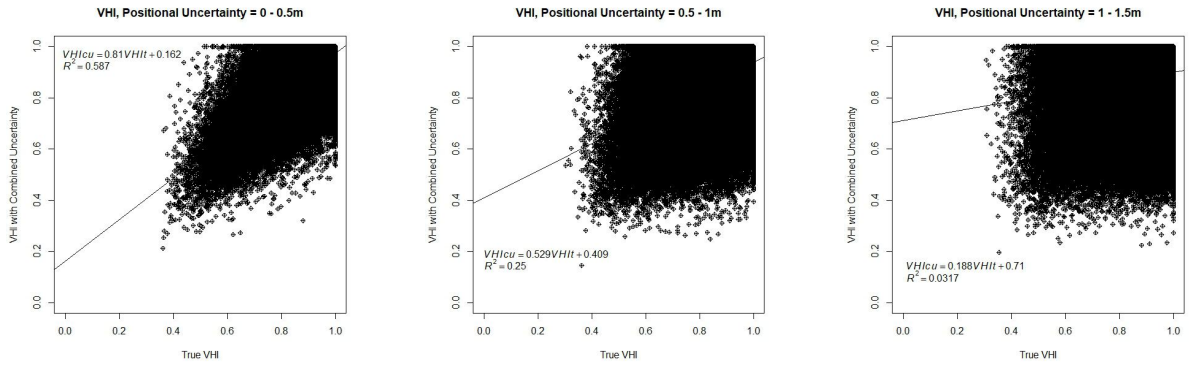

(a) (b) (c)

Figure 10: Uncertainty in VHI Resulting from the Combined Uncertainty in Planar Geolocation and Sensor Spectral Performance, Shown as a Function of Uncertainty in Planar Geolocation; (a) Planar location uncertainty in the range of 0 to 0.5-m of "true" geolocation (or 0 to 5 pixels); (b) Planar location uncertainty in the range of 0.5- to 1-m of "true" geolocation (or 5 to 10 pixels); (c) Planar location uncertainty in the range of 1- to 1.5-m of "true" geolocation (or 15 to 20 pixels)

6. REFERENCES

[1] http://AggieAir.usu.edu; April 29, 2018.

[2] Evans, H., J. Lange, and J. Schmitz. 2014. {The Phenomenology of Intelligence-focused Remote Sensing; Volume 1, Riverside Research}, New York (2014).

[3] Trishchenko, A. P., J. Cihlar, and Z. Li. 2002. Effects of spectral response function on surface reflectance and NDVI measured with moderate resolution satellite sensors. *Remote Sensing of Environment*, 81:1-18.

[4] Gonsamo, A., and J. M. Chen. 2013. Spectral Response Function Comparability Among 21 Satellite Sensors for Vegetation Monitoring. *IEEE Transactions on Geoscience and Remote Sensing*, 51(3):1319-1335.

[5] Cundill, S. L., H. M. A. van der Werff, and M van der Meijde. 2015. Adjusting Spectral Indices for Spectral Response Function Differences of Very High Spatial Resolution Sensors Simulated from Field Spectra. *Sensors*, 15:6221-6240; doi:10.3390/s150306221

[6] Holben, B. N., C. O. Justice. 1980. The Topographic Effect on Spectral Response from Nadir-Pointing Sensors. *Photogrammetric Engineering and Remote Sensing*, 46(9):1191-1200.

[7] Torres-Rua, A. 2017. Vicarious Calibration of sUAS Microbolometer Temperature Imagery for Estimation of Radiometric Land Surface Temperature. *Sensors*, 17, 1499; doi:10.3390/s17071499.

[8] Marsetič, A., K. Oštir, and M. K. Fras. 2015. Automatic Orthorectification of High-Resolution Optical Satellite Images Using Vector Roads. *IEEE Transactions on Geoscience and Remote Sensing*, 53(11):6035-6047.

[9] Ortiz, S. M., J. Breidenbach, R. Knuth, and G. Kändler. 2012. The Influence of DEM Quality on Mapping Accuracy of Coniferous- and Deciduous-Dominated Forest Using TerraSAR-X Images. *Remote Sensing*, 4:661-681; doi:10.3390/rs4030661.

[10] Aguilar, M. A., F. Agüera, F. J. Aguilar, and F. Carvajal. 2008. Geometric accuracy assessment of the orthorectification process from very high resolution satellite imagery for Common Agricultural Policy purposes. *International Journal of Remote Sensing*, 29(24):7181-7197.

[11] https://www.spectraldevices.com/products/multispectral-camera-rgb-and-nir-bands; April 29, 2018

[12] Liu, C.-C., and P.-L. Chen. 2009. Automatic extraction of ground control regions and orthorectification of remote sensing imagery. *Optical Society of America*, 17(10):7970-7984.

[13] Habib, A., W. Xiong, F. He, H. L. Yang, and M. Crawford. 2015. Improving Orthorectification of UAV-Based Push-Broom Scanner Imagery Using Derived Orthophotos from Frame Cameras. *IEEE Journal of Selected Topics in Applied Earth Observations and Remote Sensing*, 10:262-276. DOI: 10.1109/JSTARS.2016.2520929.

[14] Habib, A., Y. Han, W. Xiong, F. He, Z. Zhang, and M. Crawford. 2016. Automated Ortho-Rectification of UAV-Based Hyperspectral Data over an Agricultural Field Using Frame RGB Imagery. *Remote Sensing*, 8, 796; doi:10.3390/rs8100796.

[15] Laliberte, A. S., J. E. Herrick, A. Rango, and C. Winters. 2010. Acquisition, Orthorectification, and Object-based Classification of Unmanned Aerial Vehicle (UAV) Imagery for Rangeland Monitoring. *Photogrammetric Engineering & Remote Sensing*, 76(6):661–672.

[16] Laliberte, A., C. Winters, and A. Rango. 2008. A procedure for orthorectification of sub-decimeter resolution imagery obtained with an unmanned aerial vehicle (UAV) [abstract]. American Society for Photogrammetry and Remote Sensing Annual Conference, April 28 - May 2, 2008, Portland, OR.

[17] Jhan, J.-P., J.-Y. Rau, and C.-Y. Huang. 2016. Band-to-band registration and ortho-rectification of multilens/multispectral imagery: A case study of MiniMCA-12 acquired by a fixed-wing UAS. *ISPRS Journal of Photogrammetry and Remote Sensing*, 114:66–77.